

RSC Advances



This is an *Accepted Manuscript*, which has been through the Royal Society of Chemistry peer review process and has been accepted for publication.

Accepted Manuscripts are published online shortly after acceptance, before technical editing, formatting and proof reading. Using this free service, authors can make their results available to the community, in citable form, before we publish the edited article. This *Accepted Manuscript* will be replaced by the edited, formatted and paginated article as soon as this is available.

You can find more information about *Accepted Manuscripts* in the [Information for Authors](#).

Please note that technical editing may introduce minor changes to the text and/or graphics, which may alter content. The journal's standard [Terms & Conditions](#) and the [Ethical guidelines](#) still apply. In no event shall the Royal Society of Chemistry be held responsible for any errors or omissions in this *Accepted Manuscript* or any consequences arising from the use of any information it contains.

ARTICLE

Electrode-embedded nanopores for label-free single-molecule sequencing by electric currents

Cite this: DOI: 10.1039/x0xx00000x

Kazumichi Yokota, Makusu Tsutsui and Masateru Taniguchi

Received 00th January 2012,
Accepted 00th January 2012

DOI: 10.1039/x0xx00000x

www.rsc.org/

Electrode-embedded nanopores have been developed to realize label-free, low-cost, and high-throughput DNA sequencers and are recognized as a promising platform along with solid-state and biological nanopore devices for use in personalized medicine based on genomic information. Rapid and high-speed measurements for single nucleotide molecules are enabled through direct electrical probes and control without either amplification processes or chemical reagents. This new nanoarchitecture can sequence DNA and RNA molecules owing to the changes in the tunneling current conducted via single-base molecules passing through the nanopores. The method for controlling the translocation speed of single DNA and RNA molecules is a critical technology for reading single-base molecules with high accuracy and throughput.

1. Introduction

Genomic information is obtained by the sequencing of DNA, in which adenine always pairs with thymine, whereas guanine always pairs with cytosine. The Human Genome Project provided a complete genetic road map for the 3 billion chemical base pairs that constitute human DNA. Many expected that the end of the Human Genome Project meant the dawn of personalized medicine and therapeutics based on genomic information. However, throughput and cost of DNA sequencing are barriers to overcome.^{1,2}

First- and second-generation DNA sequencing technologies identify base molecules through light emission. They require PCR to amplify sequencing templates so that sufficient material is available for generating detectable signals. Furthermore, these sequencing technologies require fluorescent labels. In contrast, third-generation DNA sequencing technologies directly detect single-base molecules by changes in electric current,³ thus rendering PCR amplification and fluorescent unnecessary. The comparison of throughput and total cost for determining the complete human genome using DNA sequencing technologies of each generation shows that first-generation technologies take three months and cost approximately \$10 million, whereas second-generation technologies take two months and cost approximately \$0.1 million. The sequence of the complete human genome can be determined in one day for \$1000 using third-generation technologies.^{3,4}

Nanopore-based devices are critical to third-generation DNA sequencing technologies. Such nanodevices minimize the

cost of ultrahigh-speed sequencing of kilobase-length single-stranded genomic DNA or RNA or facilitate the identification of individual small molecules using only electric currents and no fluorescent labeling. Nanopore-based devices are classified as bio-nanopores and solid-state nanopores. Deamer and Branton proposed a single-molecule DNA sequencer based on bio-nanopores⁵. Bio-nanopores are formed by channel proteins with several nanometer-sized nanopores on lipid bilayers and can identify ions, small molecules, and DNA passing through the nanopores by changes in the ionic current flowing through the nanopores. Solid-state nanopores mimic bio-nanopores and are manufactured by microfabrication technologies. Typical solid devices have nanopores of several nanometers in diameter on silicon substrates covered with Si₃N₄ and SiO₂ thin films.^{6,7} Their operating principle for identifying single-base molecules is similar to that of bio-nanopores; however, the proof of concept has not been demonstrated yet.

Nanogap-embedded nanopores, which are categorized into a type of solid-state nanopores, are expected to detect molecules passing through the nanopores by changes in the electric current flowing between the nanogap electrodes and not by changes in the ionic current flowing parallel to the nanopores. The electric current passing between the nanoelectrodes originated from the tunneling current conducted via the molecules passing through the membrane. This behavior is similar to that of a scanning tunneling microscope (STM), which detects the type and number of molecules present between a substrate and the STM tip.⁸ Therefore, similar to an STM, gating nanopores can identify the type and number of single molecules passing through them. Two groups have

demonstrated the proof of concept for identifying single-base molecules via tunneling currents.^{9,10}

To realize \$1000 genome sequencers, numerous researchers have been focusing on demonstrating the proof of concept for identifying single-base molecules by changes in electric current. High accuracy and throughput for reading out base molecules are required when single-molecule technologies are applied to practical DNA sequencers. For high accuracy, DNA has to pass through the nanopores or nanoelectrodes in one direction, ideally at constant speed. In addition, considering the commercially available amplifiers where the sampling rate for measuring currents of several 10 pA is limited to 250 KHz, the translocation speed of single DNA molecules has to be reduced to 1 base/ms.¹¹ On the other hand, for high throughput, single DNA molecules have to pass through nanopores or nanogaps with high translocation speed. Consequently, we have to develop a method for controlling the translocation speed of single DNA molecules.

In this review article, for identifying single-base molecules, we focus on two core technologies that use electric signals and control translocation speed. Especially, we focus on electrode-embedded nanopores, for which the proof of concept for reading out single molecules of DNA and RNA was demonstrated.

2. Sensing principles and operation of nanopore devices

For single-molecule detection, optical imaging techniques using fluorescent probes are powerful research tools, shedding light on the function and dynamics of single molecules.¹² However,

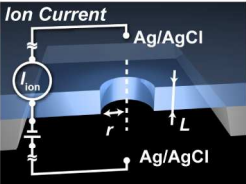
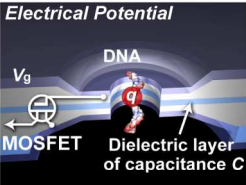
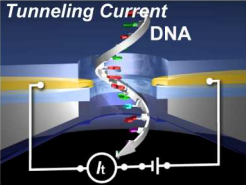
fluorescent labeling is time consuming and expensive, and data acquisition from single molecules limits the temporal resolution of detection. The use of nanopore-based devices, by which single molecules are directly detected during the passing of target molecules through a molecular-sized pore, is considered promising for label-free single-molecule detection. Furthermore, the detection of single molecules via electrical signals is expected to overcome the limitations of time resolution in the measurements, in principle, the lower limit of the thermal noise of the electrons. Thus, electrode-embedded nanopore devices demonstrate high potential as low-cost, rapid, and label-free single-molecule sensing platforms.

For nanopore technologies, DNA sequencing based on the single-molecule detection of nucleobases is a development objective. The study of solid-state nanopore technologies started with ionic current measurements, mimicking patch clamp techniques for biological systems, and then, directed the development of DNA sequencing devices on single nucleobase molecular sensitivity. Responding to this need, the probe electrodes on several recently developed nanopore devices are fabricated adjacent to a nanopore to measure the target single molecules directly. We review the electrode-embedded nanopore devices and related devices based on the signal type for electrical detection, which are ionic current, electrical potential, and tunneling current. Moreover, we cover the development stages of such nanopore devices.

2.1 Detection by ionic current

Signal sensing on solid-state nanopore devices was first

Table 2.1 Solid-state nanopore technologies for electrical sensing of DNA.

Technique	Sensing Principle	Advantage	Ref.
	<p>Exclusion of ions inside a nanopore by target molecules increases a pore resistance of $\rho L/\pi r^2$ (resistivity of solution ρ, pore length L and radius r). The electrical signals are acquired as ionic current (I_{ion}) changes by Ag/AgCl electrodes located at the top and bottom of a nanopore.</p>	<p>Simple device structure, requires only a single-molecular scale nanopore. Relatively large current can be observed, although it depends on electrolytic concentration.</p>	<p>13, 17-19 (DNA) 20 (RNA)</p>
	<p>Electrical potential change inside a nanopore by target molecules with charge q is detected as a modulation of gate voltage ($\Delta V_g = \Delta q/C$) by using a MOSFET device embedded in the nanopore.</p>	<p>High speed operation is feasible because of a high speed performance for the embedded-MOSFET. Integration with bottom-up process has been demonstrated by using such as nanowire-FET and graphene nanoribbon.</p>	<p>43,44 (DNA)</p>
	<p>Tunneling current (I) via target single molecules is detected during a translocation of those molecules. The single-molecular conductance for the target molecules is measured by a pair of nanogap electrodes embedded in the nanopore.</p>	<p>Highly spatial resolution by tunneling current is expected. DNA sensing based on single base molecule identification has been demonstrated.</p>	<p>9,10 (DNA) 74 (RNA)</p>

achieved by measuring the ionic current through a nanopore by Golovchenko *et al.*¹³ Target single molecules were detected by blocking the ionic current during the passage of molecules through the nanopores (Table 2.1: Ion Current). In a rather simplistic expression,¹⁴ the ionic current for a nanopore is limited by the nanopore size (in case of a cylinder by the cross-sectional area and length) and the resistivity ρ of the electrolyte solution. Thus, its resistance is given by $R_{\text{pore}} = \rho L / \pi r^2$. In addition, the resistance from the electrode located at an infinite distance relative to the nanopore, which is called the access resistance (R_{acc}), is $R_{\text{acc}} = \rho / 4r$. The total conductance of the given nanopore device is

$$(R_{\text{pore}} + 2R_{\text{acc}})^{-1} = \left(\frac{\rho L}{\pi r^2} + \frac{\rho}{2r} \right)^{-1} \quad (1).$$

As seen in eq. (1), the main parameters for such nanopore devices are the nanopore radius r and the nanopore length L , determined by the thickness of the freestanding membrane on which the nanopore is fabricated. When the nanopore is filled with a single molecule of cross-sectional area $\pi r'^2$ and length L , the change in the nanopore resistance is $\Delta R_{\text{pore}} = R_{\text{pore}} \times r'^2 / (r^2 - r'^2)$. The resistance change in low-aspect-ratio nanopores ($L < r$) for spherical objects was given by Bacri *et al.*¹⁵ and that in long and large pores is known as the Coulter counter method.¹⁶ In any case, because a molecule intrinsically possesses volume that excludes ions, target molecules can be sensed without labeling. The ionic current blockage of unlabeled DNA (Li *et al.*¹⁷ and Storm *et al.*^{18,19}) and RNA (Wanunu *et al.*²⁰) passing through the nanopores was investigated, and the effect of size, folding structures, and translocation time of biological polymers were identified by ionic current depression and duration time during translocation.

2.1.1 Single-molecule detection by ionic current. For detection at the single-molecule level, electrical sensitivity is enhanced by making r close to r' , and the spatial resolution is increased by decreasing L . For minimizing L , new material approaches other than the widely used SiN_x membrane on a silicon substrate, such as Al_2O_3 and graphene membranes, have attracted attention. Venkatesan *et al.* reported controlling the membrane thickness of Al_2O_3 at the angstrom level by atomic layer deposition (ALD) methods²¹. Graraj *et al.* fabricated nanopores in graphene, a single atomic layer of graphite, and measured the ionic current through the graphene nanopores.²² Despite the extreme thinness of graphene, which has an effective thickness of ~ 0.6 nm, the graphene membrane worked as a good ionic insulation layer.

Solid-state nanopore devices are fabricated by nanofabrication techniques, such as focused ion beam (FIB) and electron beam (EB) lithography, and etching. Therefore, the actual nanopore structure does not always have an ideal cylinder form. Considering the tapered structure of a nanopore and using an appropriate approximation, Kowalczyk *et al.* discussed the resistance through a more realistic nanopore structure.²³ The resistance within the equipotential spheroid

can be calculated by approximating the pore surface as a hyperboloid

$$R_{\text{pore}}^{\text{hyp}} = \frac{\rho}{\pi r} \frac{\sin \alpha}{1 - \cos \alpha} \arctan \left(\frac{\sqrt{r_w^2 - r_N^2}}{r_N} \right) \quad (2),$$

where r_w is the widest radius, r_N is the narrowest radius, and α is the angle of the asymptotic line of the hyperboloid given by $\sin^2 \alpha = r_w^2 - r_N^2 / (L^2/4 + r_w^2 - r_N^2)$. Eq. (2) well simulates the experimental ionic conductance of the nanopore. In the extreme case, the internal substructure of the nanopores, that is, the variation of the inside diameter of the nanopores, is shown as the conductance change of the ionic current trace.²⁴

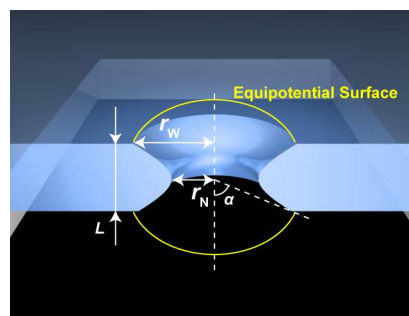


Figure 2.1.1 Hyperboloid nanopore structure for simulating the actual fabrication of nanopore devices. The yellow line shows the cross section of the equipotential spheroid, which gives an exact analytical solution.²³

As the size of a nanopore decreases to the single-molecule level, solid surfaces and solid-liquid interfaces affect the conductance (resistance) through the nanopore because of the high specific surface area of the nanopore. Ionic conductance originating as surface charges is observed as conductance saturation at low electrolytic concentrations.²⁵ Pore resistance can be written as

$$R_{\text{pore}}(\sigma) = \frac{L}{\pi r^2} \left(e(\mu_X + \mu_Y)n_{XY} + \mu_X \frac{2|\sigma|}{r} \right)^{-1} \quad (3),$$

where μ_X , μ_Y , and n_{XY} are the electrophoresis mobility of electrolyte X, electrolyte Y, and the density of XY, respectively, e is the elementary charge, and σ is the surface charge density of the nanopore. The first term of eq. (3) is equivalent to R_{pore}^{-1} in eq. (1) because ρ is defined by $[e(\mu_X + \mu_Y)n_{XY}]^{-1}$. The second term, which is dominant at low n_{XY} , represents the current produced by electroosmotic flow. In the case of nanopores fabricated on SiO_2 membranes using KCl electrolyte, the K^+ ions accumulate on the SiO_2 surface owing to the negative surface charge of $2\pi r\sigma/L$ (the value of $|\sigma|$ for SiO_2 is typically 25–60 mC/m²) from the surface-SiO⁻ groups.^{26,27} The electric field drives the accumulated K^+ ions and produces the electroosmotic flow current μ_K . Thus, $(\mu_X|\sigma|)^{-1}$ can be also referred to as the surface conductance and has values of 10^{-9} to 10^{-8} S.²⁸

Smeets *et al.* pointed out that the contribution of electroosmotic current is not negligible under the condition of $n_{XY} \times r \ll |d|/e$, although the actual situation is difficult owing to the dependence of σ on zeta potential,²³ that is, σ is not constant but depends on solid and liquid materials and n_{XY} . In experiments with nanochannels²⁶ and nanotubes,²⁹ the ionic current at n_{XY} of sub-millimolar concentration through small r less than several tens of nanometers was ascribed to an electroosmotic flow contribution.

Not only nanopore–liquid interfaces but also molecule–liquid interfaces affect the sign of ionic current change at low electrolyte concentration. Owing to the large negative charge of the phosphate backbone in DNA molecules, DNA molecules are surrounded by ions in solutions. By the inflow of solvated ions, the electrolyte density in a nanopore increases during the translocation of DNA through the nanopore. As a result, the ionic current through the nanopore increases instead of decreasing, when the counter ion contribution is more than the ion exclusion effect.^{23,30,31} Ionic current enhancement was observed for a KCl concentration of < 0.4 M. Therefore, the observed ionic current cannot always directly assign the signatures of target molecules because the structural and electrostatic properties of the nanopores affect the ionic current passing through the nanopores. For accurately describing the ionic current passing through the nanopores, He *et al.* used a multiphysics model that includes electrostatics expressed with the Poisson–Boltzmann equation, the Navier–Stokes flow motion equation, DNA motion by dragging force, and ion motion expressed by using the Nernst–Planck equation.^{32,33}

2.1.2 Operation of electrode-embedded nanopore devices for ionic current detection. In principle, at least, the electrodes for ionic current sensing need not always be proximal to the nanopores because the electric field is mainly concentrated around the nanopores owing to the large R_{pore} compared to R_{acc} . However, as discussed above, for accurately sensing at single-molecule sensitivity levels, especially for the sensing of biomolecules such as DNA and RNA, the electrostatic characteristics near nanopores strongly affect the observed ionic current signals. Additional electrodes adjacent to a nanopore enable the exploration or control of the electrostatic characteristics of nanopores; furthermore, it is also expected that such electrodes capture the signatures of molecules by directly probing the target molecules. The electrode, which is implanted in the membrane of a nanopore and is surrounded by dielectric materials, acts as a gating electrode for the ionic current passing through the nanopore. By applying a gate voltage V_g , a surface charge is induced, and counter ions start to accumulate. As a result, the conductance of nanochannels³⁴ and nanopores³⁵ is modulated by V_g at low electrolyte concentrations of less than a few millimolar.

When a nanopore-embedded electrode is in contact with an electrolyte solution, the electrode can probe the local electrical characteristics inside the nanopores.³⁶ Rutkowska *et al.* mapped the current by using the potential of two working electrodes, one outside the nanopore (WE1) and the other inside of the nanopore (WE2), and suggested that the conduction

characteristics are mapped by the current distribution in the cell rather than by the geometry or electrostatics of the nanopore.³⁷ Menard *et al.* measured the transverse ionic current by fabricating an additional short nanochannel orthogonal to the transport channel for DNA translocations.³⁸ They observed an enhancement of the transverse current at high electrolyte concentration (1 M KCl) and current depression at low electrolyte concentration (125 mM KCl) during DNA passing through the nanochannel. Wilson *et al.* theorized that single-base molecules for DNA could be discriminated by measuring the transverse ionic current via nanochannels less than 2 nm.³⁹

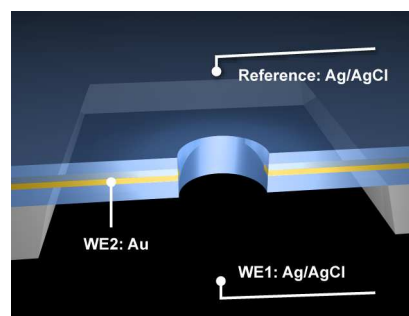


Figure 2.1.2 Schematic illustration of an electrode-embedded nanopore device for ionic current detection. The electrode is embedded into the nanopore probes to monitor the electrical characteristics inside the pore.³⁷

2.2 Detection by local electrical potential

For nanopore devices in which the operation principle is based on measuring the ionic current through nanopores, the sensing capability and spatial resolution for target molecules are limited or affected by the structure of the pores and the thickness of the freestanding membranes. By installing sensing electrodes close to a nanopore, target molecules passing through the nanopore are directly explored. Moreover, with the aid of the additional signal acquired by the embedded electrodes, a clearer signature of the target molecules is expected.

2.2.1 Single-molecule detection by local charge. By using fabrication techniques for metal–oxide–semiconductor field-effect transistors (MOSFETs), a nanopore device embedded with a thin dielectric oxide layer (< 2 nm) is produced (Table 2.1: Electrical Potential). The thin dielectric layer works as a gate capacitance of C connected to the nanopore. When a target molecule with q charge is driven into the nanopore by an external electric field, the internal charge inside the nanopore changes (Δq). Consequently, the gate voltage V_g between the metal layer (poly Si) and the semiconductor layer (Si) varies. In the simplest model,⁴⁰ ΔV_g and Δq are related as follows:

$$\Delta V_g = \frac{\Delta q}{C} \quad (4)$$

Many biomolecules such as proteins, DNA and RNA are soluble in polar solvents (e.g., water) and are polar in nature. Actually, DNA and RNA are highly negatively charged polymers owing to the phosphate backbone. Furthermore, individual base molecules are identifiable by the charge

distribution of the electrical dipole moment for each molecule.^{41,42} Thereby, DNA molecules are detectable without being labeled.

2.2.2 Operations of FET-embedded nanopore devices.

Heng *et al.* reported charge detection on DNA by fabricating MOS–capacitor-embedded nanopore devices.⁴³ They performed simultaneous measurements of ionic current depression and voltage change during the translocation of 150 base pair (bp) DNA through the nanopore. Here, it was pointed out that the oscillations on the recorded voltage change were attributed to the charge on the DNA. Although the signals of each oscillation experimentally observed have not been assigned to each 150 bp in the DNA, in other words, although the detection on single-base molecule sensitivity has not been demonstrated, theoretical calculations based on molecular dynamics (MD) simulations^{43–45} and circuit simulations⁴⁶ predicted the possibility of detection at the single-base molecular level.

The advantage of MOS-based nanopore devices is that the integrated MOSFET device located close to the nanopore can detect ΔV_g . In on-chip-integrated devices, the parasitic capacitance between the sensing and detection parts needs to be reduced; hence, high-speed measurements are expected by taking advantage of the intrinsic high-operation speed of FET devices (\sim GHz).⁴³

Not only top-down techniques but also bottom-up approaches were demonstrated in FET-integrated nanopore devices. Xie *et al.* used a Si nanowire synthesized by chemical vapor deposition (CVD) methods as a FET channel for detecting local electric potential.⁴⁷ After making source–drain contacts with the nanowire on a SiN_x membrane, a nanopore was formed on the membrane by using a focused electron beam through the edge of the nanowire. FET signals associated with DNA translocation are recorded as channel conductance changes, when an ionic strength gradient is imposed across the nanopore.

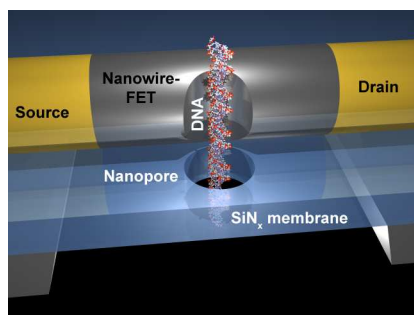


Figure 2.2.1 Schematic illustration of an FET-embedded nanopore device. The change in local potential is detected through the Si nanowire FET synthesized by bottom-up processes.⁴⁷

Moreover, the use of graphene sheets in integrated nanopore devices was proposed and examined^{48,49} because zero-gap semiconductors and extremely thin materials are recognized as promising materials for nanopore devices. The theoretically predicted operation principle was that of the energy level

modulation of the quantized conductance in the graphene channel, originating at the coupling with the molecules proximal to the energy state⁵⁰ and edge states on graphene.⁵¹ The fabrication of a device based on graphene nanoribbon (GNR) nanopores was demonstrated as follows: 1) a graphene sheet synthesized by CVD methods is transferred onto the SiN_x membrane and patterned to a GNR shape by EB lithography; and 2) a nanopore is formed on the membrane by using a focused electron beam through the edge of the GNR, similar to the fabrication of nanowire–nanopore devices.

Nanopore devices using FETs exhibit large transverse currents on the order of nanoamperes to microamperes through the FET channels compared to the tunneling current (on the order of picoamperes, as discussed in the next section) passing through the molecules, which enables the detection of signals from the target molecules.

2.3 Detection by tunneling current

The transverse current in a nanopore can be measured by a pair of electrodes embedded in the nanopore. Target molecules connected to these two electrodes through electrolyte solutions are sensed by ionic current depression or enhancement during translocation in the nanopore, as described in section 2.1.2. When the gap distance between these two electrodes is sufficiently small to permit electron tunneling via target molecules, the tunneling current conducted by target single molecules can be observed (Table 2.1: Tunneling Current).

2.3.1 Single-molecule detection by tunneling current.

For the electrical conductance at the single-molecule scale, the electrical transport mechanism is expressed by the quantum conductance regime better than ohmic conduction in a bulk system. When the dimension of a given system is smaller than the mean free path of an electron, the electrons are transported without being scattered. The conductance through a transparent conductive channel is given by $G_0 = 2e^2/h \approx 77.5 \mu\text{S}$, where h is the Planck constant. By inserting a molecule with finite transmission probability (T_e) between the electrodes, the tunneling conductance I_t/V is expressed as

$$I_t/V = \frac{2e^2}{h} T_e \quad (5).$$

As the transmission probability of the molecule depends on its own electronic states and the coupling with the electrodes, the molecular species between the electrodes are identified by the electrical conductance without labeling.

The transmission probability of electrons transported via the molecule between two electrodes (hereafter, referred to as 1 and 2) can be theoretically calculated using Green's function and expressed as

$$T_e = \text{Tr}[\Gamma_1 G \Gamma_2 G^\dagger] \quad (6).$$

Green's function G is $G(E) = (ES_M - H_M - \Sigma_1 - \Sigma_2)^{-1}$ from the overlap and the Hamiltonian matrices of the molecule S_M and H_M , where $\Gamma_{1(2)}$ can be written as $\Gamma_{1(2)} = i(\Sigma_{1(2)} - \Sigma_{1(2)}^\dagger)$ by using

the self-energy terms $\Sigma_{1(2)}$. For weak coupling, the conductance of the tunneling current through a single energy level E_N in the limit of zero bias is approximately given as

$$I_t / V \approx \frac{e^2}{\pi\hbar} \frac{\Gamma_1 \Gamma_2}{(E_F - E_N)^2} \quad (7),$$

where E_F is the Fermi level of the electrodes.

From theoretical calculations by using the Green's function method, Zwolak *et al.* predicted the possibility of single-base detection for DNA by measuring the tunneling current via base molecules.⁵² They demonstrated that each base molecule has a distinguishable tunneling current owing to the difference of the energy level of the highest occupied molecular orbital (E_{HOMO}) or that of the lowest unoccupied molecular orbital (E_{LUMO}) of base molecules, relative to E_F . This can be understood by considering the term $(E_F - E_N)$ in eq. (7) by substituting $E_{\text{HOMO(LUMO)}}$ into E_N . Moreover, the predicted tunneling current signatures of base molecules are sufficiently independent of the nearest-neighbor base molecules for allowing assignment.⁵³ This means that DNA scanning by tunneling current allows the sequential readout of nucleobases at the single-molecule scale. Actually, with the aid of the strong dependence of tunneling current I_t on distance d , which is expressed as $I_t \propto \exp(-2kd)$ and by using the decay constant k , high-spatial-resolution measurements at the single-base molecule scale were established. Tanaka *et al.* showed images of single DNA at the base molecular scale by using STM.⁵⁴ Although the strong current dependence on distance increases the distribution of the current magnitude by taking advantage of the DNA structural changes,^{55,56} it is predicted that the tunneling current identification of the DNA base molecules is feasible by using the bandwidth and applied electric field in the measurements.^{57,58}

Theoretical approaches are also used to search for materials for nanopore devices by using tunneling current detection. Metallic materials such as Pd,⁵⁹ TiN,⁶⁰ carbon nanotube,⁶¹ and graphene,^{62,63} were investigated.

2.3.2 Operation of electrode-embedded nanopore devices and tunneling current detection. For tunneling current detection in nanopore devices, nanogap electrodes should be embedded in the nanopores. Nanogap electrodes embedded in nanopores were fabricated by EB lithographic techniques,^{64–67} FIB and EB⁶⁸ and EB-induced deposition (EBID).⁶⁹ In spite of the progress in nanofabrication, precise and highly reproducible fabrication on the order of 1 nm gap, which is comparable to nucleotide spacing of 0.7–0.9 nm,⁷⁰ remains a challenge. An ingenious way to overcome processing accuracy limits is the widely used break-junction (BJ) methods. In these methods, gap electrodes are formed by breaking metal contacts mechanically or physically. In the STM–BJ method,⁷¹ an STM measurement system is used, and gap electrodes are formed between the metal substrate and metal tip. Moreover, by pulling the metal wire to opposite directions, the metal wire breaks and two facing gap electrodes form. This mechanical operation is referred to as the mechanically controllable break-

junction (MCBJ) method; in this method, a freestanding wire with ends that are fixed on a bending beam with three-point bending configuration.⁷² BJ methods provide distance-adjustable gap electrodes at the angstrom scale by piezoelectric actuation, and thousands of gap formation trials are tested by approaching and retracting the electrodes repeatedly. A large amount of data acquired by repetitive measurements facilitates the statistical analysis of the signals with some degree of distribution.

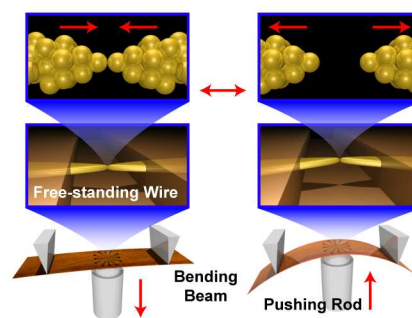


Figure 2.3.1 Schematic illustration of the formation of nanogap electrodes by the MCBJ method. The gap distance at the single-molecule scale is adjusted using the three-point bending mechanism.¹⁰

By using nano-MCBJ, which combines nanofabrication techniques and MCBJ for enhancing mechanical stability and controllability, Tsutsui *et al.* measured the tunneling current passing through DNA nucleotide molecules and demonstrated the identification of single nucleobase molecules.¹⁰ Detection by tunneling current identification is a powerful method to identify chemically modified nucleobases and normal nucleobases because chemical functional groups modulate $E_{\text{HOMO(LUMO)}}$ of nucleobases by themselves without additional labeling. The tunneling current identification of methyldeoxycytidine and 8-oxo-deoxyguanosine was reported.⁷³ The analysis of these types of DNA modification, which is critical to the epigenetic mechanism of various important biological processes, such as genetic expressions, replications, and aging, and the difficulty in broad identification by universal biomolecular recognition, would be an important target for solid-state nanopore devices.

Other major challenge in the development of nanopore devices for single-molecule detection of nucleobase molecules is the sequential sensing of nucleobase molecules, in other words, DNA and RNA sequencing with single-molecule sensitivity. By assembling partial sequences in randomly detected RNA using nano-MCBJ, Ohshiro *et al.* showed that the resequencing of 7-mer RNA was possible.⁷⁴ For the unified treatment of the tunneling current in nucleobase molecules measured under different conditions between controllable nanogap electrodes, they utilized the relative conductance values of four types of ribonucleoside monophosphate (rXMP: X = A, adenosine; C, cytosine; G, guanosine; T, thymidine). The relative conductance values were identified by attributing the largest conductance peak to rGMP because the guanine

molecule exhibits the largest tunneling conductance. DNA sequencing can be also assigned in the same manner by comparing the relative conductance ratios of four deoxyribonucleoside monophosphates (dXMP: X = A, adenine; C, cytosine; G, guanosine; T, thymidine). The observed conductance values and ratios are summarized in Table 2.2.

Table 2.2 Single-molecule conductance of nucleotides

Nucleotide	Conductance (pS)	Relative Ratio to Guanine
rGMP	122.7	1
rAMP	92.0	0.75
rCMP	64.1	0.52
rUMP	50.0	0.41
dGMP	86.7	1
dAMP	66.8	0.77
dCMP	59.5	0.69
dTMP	39.1	0.45

RNA and DNA nucleotides are represented as rXMP and dXMP, respectively.

Ideally, sequencing is performed by the nanogap electrodes embedded in the nanopore that guides and regulates the passing of DNA chains, as seen in 2.3.1. Tsutsui *et al.* also reported the fabrication of nanopore devices with embedded nanogaps, formed in SiO₂-sandwiched Au by an electrical BJ method. By using these devices, they demonstrated the identification of base molecules in DNA oligomers.⁷⁴ We point out that the further regulation of molecular configurations by small nanopores appropriate to molecular sizes is essential for accurate measurements. In addition, the regulation of the traveling direction of DNA or RNA chains, seen in biosystems, is necessary for reading the repeated sequences. These would be future challenges in the development of solid-state nanopore devices.

3. Translocation speed control of single molecules in nanopores and nanochannels

As described in the previous section, recent studies have proven the potential of the transverse electron transport approach based on either tunneling current,^{10,39,52,53,69,73,74,75,76,77} ionic current,^{78,79,80,81,82} or surface charge-modulated current measurements,^{47,48,83} for the label-free identification of single-molecule DNA in liquid media. Besides proof-of-principle verifications, it is of practical importance to understand and control the dynamic motions of molecules in solution to make use of the promising single-molecule sensing capability in genome sequencing.^{11,84,85} This is not only critical for electrode-embedded nanopores, but also in solid-state nanopore sensing as a whole, owing to the fact that the electrophoretic translocation of DNA molecules is fast, typically around 10 base/ μ s (10^3 - 10^4 times faster than the case of bio-nanopores),¹¹ because of the significantly high electric field inside the pore.^{86,87,88,89,90,91,92} For example, tunneling current flowing through single nucleotides is on the order of 10 pA,^{10,77} indicating that only several electrons are allowed to transmit through each nucleotide of the fast-moving DNA. As there is no current amplifier having sufficient gain and bandwidth to

measure such a small current change within the critically short amount of time, there is an obvious need for slowing down the molecule threading through a nanopore. Moreover, the difficulty lies in that it requires DNA to overcome the energetic barrier due to electroosmotic drag and geometrical restrictions and then enter and pass through the confined nanospace.⁹³ Therefore, translocation speed cannot be simply lowered by only decreasing the electrophoretic voltage but calls for additional means to tailor the relevant properties for manipulating the biopolymer motions while also considering its influence on the electrical signatures for single-nucleotide identification.^{84,85} Here, we review some of the state-of-the-art technologies based on solid-state nanopores aiming to regulate the motions of electrophoretically-driven polynucleotides and fulfill the requirement for nanopore sequencing with an emphasis on their compatibility with the tunneling current method, wherein electrical noise and crosstalk would emerge as additional concerns.

3.1. Advanced technology for DNA translocation speed control

Nanopores serve not only as a useful platform for detecting and identifying small objects in a liquid from their size differences via the resistive pulse technique but also as speedometers capable of quantitatively estimating the average translocation speed by measuring the time-of-flight of DNA through the pore.⁹⁴ This valuable function has actually been leveraged in studying the translocation dynamics of biopolymers and assessing the efficacy of external probes incorporated to affect their motions in a nanopore. These include electrical, optical, magnetic, and entropic forces directly or indirectly imposed on polynucleotides. In addition, there were efforts to slow down translocation by increasing solution viscosity. Ion concentration gradient and mobility were also found useful in braking DNA in a nanopore. Alternatively, and more primitively, it was demonstrated that a biopolymer can be clogged in a nanopore by making its diameter comparable to the size of the molecule. Below, we describe the efficiencies of these strategies and discuss their compatibility with the tunneling current approach.

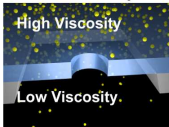
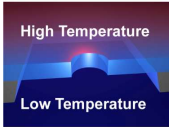
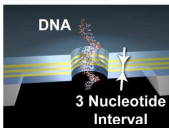
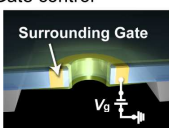
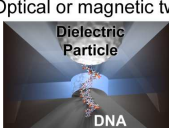
3.1.1. Environmental control of DNA mobility. Early studies have investigated the influence of solution viscosity on DNA translocation through nanopores in attempt to moderate the high-speed feature as one would expect the more viscous the solution, the larger the hydrodynamic dragging force subjected on DNA that would contribute to diminish the electrophoretic mobility. The experiments by Fologea *et al.*⁹⁵ proved the efficiency of this bulk approach. They conducted a systematic evaluation of DNA translocation speed in a silicon nitride nanopore under various viscosity conditions. Two approaches have been examined to enhance the solution viscosity: adding glycerol to the buffer or lowering the liquid temperature. As theoretically expected, the time-of-flight was found to scale linearly with the viscosity, leading to more than a factor of 5 decrease in the translocation speed by addition of glycerol for up to 50 %. Temperatures can be an alternative means to alter the liquid viscosity. Though less pronounced

than the results in a biological nanopore, this was also found effective to reduce the DNA velocity by 50 % through lowering the solution temperature from 22 to 4 degrees Celcius (Table 3.1: Solution viscosity).⁹⁵

A disadvantage in the above approach is the concomitant

influence on the ion current through the pore. Higher viscosity leads to lower solution conductivity, and hence the resistive pulse signals become weakened. Temperature affects the ion transport characteristics in more complicated way as it not only changes the liquid viscosity but also modifies the properties of

Table 3.1 Solid-state nanopore technologies for DNA translocation speed control.

Technique	Control parameter	Test conditions <i>Nanopore material and size</i> <i>Target DNA</i> <i>Salt solution condition</i> <i>Electrophoretic voltage</i>	Efficiency <i>Translocation time increase</i> <i>(Condition)</i>	Ref.
<i>Passive control</i>				
Solution viscosity 	Addition of viscous liquid (Glycerol) to buffer	4-8 nm SiN (280 nm thick) 3 kbp DNA 1.5 M KCl-TE 120 mV	5 (x5 viscosity)	95
Salt gradient 	Salt concentration difference between the solution in cis and trans	3.5 nm (25 nm thick) 2 kbp DNA 1 M KCl-10 mM Tris-HCl 300 mV	3.5 (1 M KCl in cis and 0.2 M KCl in trans)	99
Thermophoresis 	Temperature gradient across a nanopore	NA	NA	103
Functionalized nanopore 	Chemical interaction between DNA and functional molecules decorated on nanopore wall surface	3-5 nm Pb/SiN (28 nm thick) 63 nt ss DNA 1 M KCl-1mM phosphate buffer 80 mV	13 ~ 25 (4(5)-(2-mercaptoethyl)-- 1H-Imidazole-- 2-carboxiamide)	108
DNA transistor 	Electrostatic trapping forces on DNA in triple-layered metal electrodes	2 nm SiO ₂ 20 nt ss DNA 0.1 M NaCl 6.25-93.75 mV/nm	Base-by-base ratcheting (Trapping voltage 2 V; Electrophoretic force ≤ 75 pN)	112
<i>Active control</i>				
Gate control 	Nanopore surface charge state modulation by gate voltage (V _g)	< 20 nm SiO ₂ in SOI wafer 2.8 kbp DNA 1 M KCl-TE 150 mV	20 (+0.6 V gate voltage)	118
Optical or magnetic tweezer 	Position and intensity of focused laser beam on a DNA-coated particle	6-15 nm SiN 48.5 kbp λ-DNA 1 M KCl-TE 30 mV	30-nm-scale ratcheting (Optical stiffness 55 pN/μm)	120
Hydropressure control 	Hydropressure antagonizing the electrophoretic force	10 nm SiN (80 nm thick) 3.27 kbp DNA 1.6 M KCl-TE -90 mV	8 (100 mV versus -90 mV with 2.44 atm hydro- pressure)	122

DNA. As a result of the higher counter-cation density on DNA inside a nanopore at a low temperature, the blockage current reduces while the open pore current remains the same.⁹⁵ Therefore, there is a tradeoff in the viscosity approach in that the higher electrophoretic voltage may be necessary to keep the resistive pulse signals discernible from the noise, which will compensate the DNA translocation speed reductions.

While these drawbacks would be crucial in the resistive pulse technique, they are probably not so important in the tunneling current approach. Above that, we can expect suppression of thermal fluctuations of DNA molecules and Johnson-Nyquist noise that may provide a better platform for the sequencing purpose.

3.1.2. Salt gradient approach. In the nanopore sensing of DNA, electrolyte solutions are used to gain a sufficient level of ionic current for detecting its translocation through the temporal blocking of cross-membrane ion transport. Previous experiments have shown that the translocation speed of polynucleotides is insensitive to ion concentrations as long as the Debye layer is negligibly thin.^{95,96} In contrast, it was reported that DNA translocation velocity could be delayed by imposing an ion concentration gradient across a nanopore.^{97,98} Wanunu *et al.*⁹⁸ adjusted the KCl concentrations at the *cis* and *trans* to 1.0 M and 0.2 M, respectively. The five-fold asymmetric salt distributions increased the duration time of 2000 bp DNA passing through a 3.5 nm nanopore by a factor of 3.5 (Table 3.1: Salt gradient). Furthermore, this simple yet effective approach for slowing down translocation dynamics had an additional outcome: the enhancement of the capture efficiency of DNA in the pore⁹⁸ that is important from the viewpoint of sequencing throughput. Generally, the decrease in translocation speed and increase in the capture rate are paradoxical because the facilitated molecular capture naturally indicates the existence of a driving force that pulls polynucleotides into the pore, which would also act to accelerate the molecule as it passes through it. For instance, the increase (decrease) in the electrophoretic voltage will enhance (diminish) both DNA translocation speed and capture rate.

Theoretically, the intriguing function of the cross-membrane salt gradient was attributed to two factors: 1) osmotic flow⁹⁹ and 2) ion accumulation at the pore orifice.^{100,101} The former considers hydrodynamic dragging by osmotic-pressure-induced water flow from *cis* to *trans*. The model quantitatively reproduced the enhanced capture rate by the salt gradient.⁹⁹ However, it remains to be explained why translocation speed could be decreased by the osmotic mechanism, which essentially predicts the induction of fluid flow along the ion concentration gradient. On the other hand, the latter could demonstrate two conflicting effects at the same time.^{100,101} He *et al.*⁹¹ simulated the ion distribution in a biased nanopore with a salt gradient and observed cations accumulating at the pore mouth. They attributed it to the positive potential that an electric field creates to pull DNA into a nanopore, thus increasing DNA capture rates. Simultaneously, the high concentration of cations generates electroosmotic flow inside the pore in a direction opposite to

the electrophoresis of DNA, thereby decreasing translocation speed.¹⁰¹

The passive way of controlling the molecular translocation speed via the salt gradient may not interfere with transverse tunneling current measurements, let alone the possible influence of the transverse electric field on the cation distribution. As one only needs to prepare electrolyte solutions with different salt concentrations, it is worthwhile to incorporate this method in DNA detection using electrode-embedded nanopores.

3.1.3. Thermophoresis. Akin to the role of electrostatic potential gradient in electrophoresis, temperature gradient is also a driving force that moves objects in a specific direction.¹⁰² This thermophoresis was theoretically verified to be useful in threading DNA through a nanopore.^{103,104} It exploits the difference in the conformation degrees of freedom, or Gibbs enthalpy, of a long strand of DNA in high- and low-temperature regions. By employing a low thickness-to-diameter ratio pore architecture, the temperature gradient near the nanopore orifice can be made sufficiently large for DNA Gibbs free energy to vary along the temperature gradient, and thus, it is allowed to enter the pore.¹⁰³ Inside the nanopore, the polynucleotides will be further driven thermophoretically by the temperature gradient, but the effect weakens in the capture stage owing to the smaller Gibbs energy density in the 2 nm diameter cylinder than that in the exterior regions. As a result, the temperature gradient at a nanopore can effectively facilitate DNA capture via the thermophoretic mechanism while moderately increasing translocation speed compared with electrophoresis (Table 3.1: Thermophoresis).¹⁰³ It has also been suggested that the local heating of the nanopore volume would enable the stretching of DNA during translocation.¹⁰³

Another important aspect of thermophoretic control is the possible application for the denaturation of double-stranded (ds) into single-stranded (ss) DNA, a vital requirement for any type of nanopore sequencing. This can be simply accomplished by increasing the temperature of the hot side to the melting point of the dsDNA of interest. Furthermore, the difference in the Kuhn length of dsDNA and ssDNA condenses the folded conformations more. As a result, the Gibbs free energy of ssDNA is more sensitive to temperature; thus, it is more feasible to attain thermophoretic control for ssDNA by a smaller temperature gradient than for dsDNA.¹⁰³

Whether thermophoresis becomes a useful tool in nanopore sensing relies on the development of membranes with excellent thermal insulating properties. Dielectric materials commonly used as membranes, such as SiO₂ and SiN, are too conductive. Heat management can be undertaken by using resistive heaters microfabricated on a pore device. High temperature will result in increased Johnson-Nyquist noise in the transverse current. Nonetheless, if thermophoresis alone can let DNA flow through an electrode-embedded nanopore, it will be of a significant benefit as the voltage-free procedure can avoid crosstalk issues and above all would enable the denaturation of dsDNA.

3.1.4. Functionalized nanopore. Tailoring the surface chemistry by coating a solid-state nanopore with organic

molecules, which was the approach applied to protein analysis in the first place,¹⁰⁵ was also found promising for slowing down the DNA translocation. SiN nanopores, widely used for single-molecule DNA detections, possess negative native charges on the surface in a wide range of pH around 7,¹⁰⁶ which induces electroosmotic flow in a direction opposite to the translocation of the negatively charged polynucleotides. Anderson *et al.*¹⁰⁷ coated the SiN nanopore by amino-group-containing siloxanes. The amine-modified pore could prolong the 4 kbp dsDNA translocation duration by up to a factor of 4 in spite of the mitigated electroosmotic dragging in there (Table 3.1: Functionalized nanopore), which was verified by the increased electrostatic interaction of the positively charged molecules on the wall at the pH conditions of the test.¹⁰⁷

Functionalized nanopores have also been applied to ssDNA. Krishnakumar *et al.*¹⁰⁸ employed a molecule with functional groups designed to form specific chemical links with nucleotides for single-nucleotide identification by recognition tunneling. They showed an increase of two orders of magnitude in molecular translocation through a nanopore formed in a Pb/SiN membrane by decorating the top metal surface with this functional molecule.¹⁰⁸

3.1.5. DNA transistors. The controlled ratcheting of DNA at the angstrom scale is ideal for single-molecule manipulation in nanopore sequencing by tunneling current because each base molecule would be made to reside precisely in the electrode gap. This idea has actually been realized in biological nanopores by incorporating an enzyme motor for trapping and unzipping DNA at the vicinity of the pore and making full use of base-by-base replication processes by using a polymerase to displace the molecule by several angstroms per enzymatic reaction, which accomplishes an extraordinary slow translocation speed of 40 nts/s or lower.^{108,109,110}

Single-molecule ratcheting has also been pursued in solid-state devices. Stolovitzky *et al.*^{111,112} proposed applications of two opposing electrostatic fields to electrically trap DNA in a solid-state nanopore. The conceptual device architecture consists of a cylindrical nanohole sculpted in three planar electrodes equally separated by thin dielectric layers. The gap distance between the electrodes, or the thickness of the insulating layer, is set to 2.5 multiplied by the spacing between each phosphate in ssDNA. The ingenious design of an electrode-embedded nanopore was demonstrated by using molecular dynamics simulations to electrophoretically drive DNA ratcheting motions at the single-base level (Table 3.1: DNA transistor). The underlying mechanism was attributed to the electrostatic field between the electrodes, which induces an equal amount of forces that locally pull the DNA apart and virtually trap the molecule when the same number of phosphates reside in the two electrode gaps. This force balance changes upon displacing the molecule in one direction as it results in a different number of phosphates in the insulating layers. The important feature here is that the resulting local force occurs in a direction opposite to molecular displacement, thereby creating an electrical trap for single-base ratcheting.^{111,112}

Additional advantages of this so-called DNA transistor include the stretching of ssDNA via local electrostatic forces and the strong suppression of stochastic motions in a nanopore.¹¹³ Both would facilitate single-nucleotide identification by tunneling current measurements. From the viewpoint of the single-molecule manipulation method for sequencing by transverse electron transport, it would be technically possible to integrate tunneling current sensing nanoelectrodes into the DNA transistor. To make the device functional, the middle electrode in the DNA transistor can be then replaced by a pair of electrodes with a 1 nm gap.

3.1.6. Gate control for nanopore wall surface charges. When a dielectric material is immersed in water, chemical reactions occur on the surface under certain pH conditions and induce charges. As a result, an electric field causes the migration of mobile counterions near the dielectric surface and creates fluid flow along the ion stream. This electroosmotic flow is an important factor for the DNA capture and translocation in a solid-state nanopore as long as the electrophoretic voltage is used to drive the molecule into the pore.

There is an idea to electrically modulate the surface charges on a nanopore wall through a gate dielectric to fine-tune the direction and magnitude of the electroosmotic flow via the gate voltage.^{114,115,116} By doing so, we can expect two outcomes in terms of DNA translocation control. A positive gate voltage generates anionic electroosmotic flow in a direction parallel to the electrophoresis of DNA, which facilitates the polynucleotides to overcome the energy barrier and enter the pore. Conversely, negative field reverses the fluid stream bringing hydrodynamic drag force for decelerating DNA motion. At the same time, the gate effects cause two side effects. Once captured into a nanopore under positive gate voltage, DNA accelerates by electroosmotic flow, resulting in a higher translocation speed. On the other hand, the fluid flow caused by the negative gate would hinder DNA to enter a nanopore.^{114,115,116}

Gate control has been recently incorporated in nanopore sensing.^{67,78} Yen *et al.*¹¹⁷ fabricated a surrounding gate with SiO₂ nanopores of diameter 22 nm on a silicon-on-insulator wafer. By imposing positive gate voltage, it was observed that the DNA translocation speed was reduced by a factor of up to 20 (Table 3.1: Gate control). Although measurements under negative gate voltage were not reported to date, perhaps owing to the blocking effects of DNA capture, which makes it difficult to evaluate the efficiency, the gate effect was in fact opposite to theoretical expectations. This was attributed to the electrostatic interaction between the positive dielectric surface and the negatively charged DNA in solution, which attracts and traps polynucleotides on the pore wall once they come close to each other, as seen in other experiments.¹¹⁷ Therefore, it is challenging to switch the gate voltage sign from positive to negative right after every each DNA capture event.¹¹⁵

From a device fabrication viewpoint, it would not be difficult to integrate a surrounding gate at above or below the electrodes embedded in a nanopore. However, adding another

electric field in addition to the electrophoretic and transverse counterparts may lead to interferences that affect the tunneling current signals in an unpredictable fashion.

3.1.7. Optical and magnetic tweezers. The use of optical tweezers is established for single-molecule manipulation and force spectroscopy.¹¹⁸ In this method, a focused laser beam is used to 3D-trap a dielectric particle with the analytes of concern chemically attached on the surface. Keyser *et al.*¹¹⁹ applied the optical approach to demonstrate the single-molecule ratcheting of λ DNA in a SiN nanopore. To optically trap a DNA-tagged polystyrene microbead near the nanopore, the electric field across the membrane was used to electrophoretically capture the polynucleotides anchored to the micrometer-scale particle. They observed DNA entering the nanopore one-by-one from the stepwise decrease in the cross-pore ionic current. The position of the DNA residing in the nanopore was also controlled via the optical manipulation of the bead at a resolution of 30 nm, which enabled, although not at single-base resolution, the ratcheting of the biopolymer (Table 3.1: Optical or magnetic tweezer). It was also demonstrated that similar results could be obtained by using magnetic forces to trap an anchor particle.¹¹⁹

This experimental design is a concept quite different from the efforts to retard the fast translocation of DNA passing through a nanopore. The motions of one-end-fixed polynucleotides inside a nanopore can be possibly frozen by imposing a strong electrophoretic force to stretch them without letting them flow through it.^{119,120} Thereafter, their position will be fine-tuned by the electrophoretic voltage, and to a certain extent, by choosing optimal conditions for optical trap stiffness.^{119,120} The electrical strategy may not be compatible with resistive pulse sensing, as the blockage current would also be affected by the electrophoretic voltage, it would be useful in the tunneling current approach except the possible crosstalk between longitudinal and transverse charge transport. An expected problem is local heating by laser irradiation that may augment the electrical noise in the tunneling current, which can be circumvented by using magnetic tweezers. Other technical difficulties, such as the prevention of multiparticle trapping and damage by the laser beam, should also be resolved for better controlling single-molecule translocation by optoelectrical methods.

3.1.8. Hydropressure dragging. Hydropressure also facilitates or hinders DNA translocation.^{121,122} Lu *et al.*¹²² demonstrated that the translocation speed of relatively short (3.27 kb) DNA can decrease by an order of magnitude by applying hydrostatic pressure to mechanically induce fluid flow in a direction opposite to that of electrophoresis (Table 3.1: Hydropressure control). The result of pressurizing the pore is that the resistive pulse signal duration will be extended without sacrificing the signal-to-noise ratio, which is the tradeoff for lowering the electrophoretic voltage to slow down translocation. In addition, applications of pressure can expand the sensing capability of nanopores to detect even electrically neutral analytes.¹²²

The advantage of applying pressure and compensating the field acceleration of DNA to preserve the signal-to-noise ratio in ionic current measurements cannot benefit the tunneling current approach. However, it will be useful if polynucleotides can flow through a nanopore by only applying pressure because the possible crosstalk between the longitudinal and transverse electrodes can be completely eliminated. Yet, there is difficulty in mechanically driving a relatively long DNA molecule to overcome the entropic barrier and enter the pore, and subsequently modulate translocation speed, as it would require high precision and short response time, which is difficult to achieve when mechanically controlling hydrostatic pressure.

3.2. Other methods?

As described above, the technical difficulty in piercing a one-dimensional biopolymer through a confined nanospace and manipulating translocation motions constitutes a major obstacle toward realizing genome sequencing via transverse current measurements of single-stranded DNA passing through an electrode gap between the embedded electrodes in a nanopore. Additional concerns arise when voltage is used to drive DNA motion because of the interference between the electrophoretic and transverse electric fields, which complicate the interpretation of the obtained electrical signatures. Besides translocation speed control, it is also crucial to mitigate the stochastic motions of DNA in a nanopore to read out the base sequence with accuracy, similar to any single-molecule analysis. Perhaps, a promising strategy for satisfying these requirements is to take advantage of spatial confinements. As demonstrated in recent experiments,^{123,124,125,126} the speed of DNA molecules would substantially decrease down to 1 nt/2 ms or they would be trapped in a nanopore when their size is smaller than the diameter of the biopolymer.^{123,124} Molecular dynamics simulations also predict that the electrical permeation of DNA in molecular-sized pore results in the stretching of the biopolymer.¹²³ By switching off the electrophoretic voltage after driving a polynucleotide into an electrode-embedded nanopore, the DNA is expected to be immobilized between the sensor probes with a stretched conformation by making the gap size slightly smaller than the molecule. Thereafter, DNA can be moved forward or backward by adding an electric field along the pore, in the form of voltage pulse, for example. Such features would greatly facilitate single-nucleotide identifications as Brownian motions are suppressed, and there will also be no interference between the longitudinal and transverse fields. Although it is still a formidable task to fabricate DNA-sized electrode-embedded nanopores, such device architecture would provide a simple means for ratcheting single molecules and aid in the realization of nanopore sequencing.

Conclusions

We reviewed two core technologies for single-molecule electrical sequencers, single-molecule identification technologies via electric currents and methods for controlling

the translocation speed of single molecules. To date, single-molecule identification technologies have achieved DNA and RNA sequencing, and the translocation speed can be controlled by passive and active control methods. The next challenge for developing label-free, high-throughput, and high-accuracy DNA sequencers lies in the integration of the two core technologies on single devices. From the viewpoint of integration, nanopore devices can benefit from semiconductor technologies of the last 40 years because the developed microfabrication technologies can realize large-scale integrations. In particular, electrical speed control methods can be smoothly integrated to single devices. Furthermore, when single-molecule electrical sequencing technologies are applied to practical sequencers for use in medical science and clinical practice, the sequencers need to determine sequences of DNA and RNA extracted from blood and saliva. To realize smart sequencers, we need to develop pretreatment devices, where double-stranded DNA molecules are extracted from cells and tangled double-stranded DNA molecules are untangled. In addition, double-stranded DNA molecules are denatured to form single-stranded DNA molecules and guided to nanopore devices using pretreatment devices. Ideally, single-molecule DNA sequencers are expected to integrate the two core technologies and pretreatment devices onto single chips.

Acknowledgements

This study was supported by the Japan Society for the Promotion of Science (JSAP) through its "Funding Program for World-Leading Innovative R&D on Science and Technology."

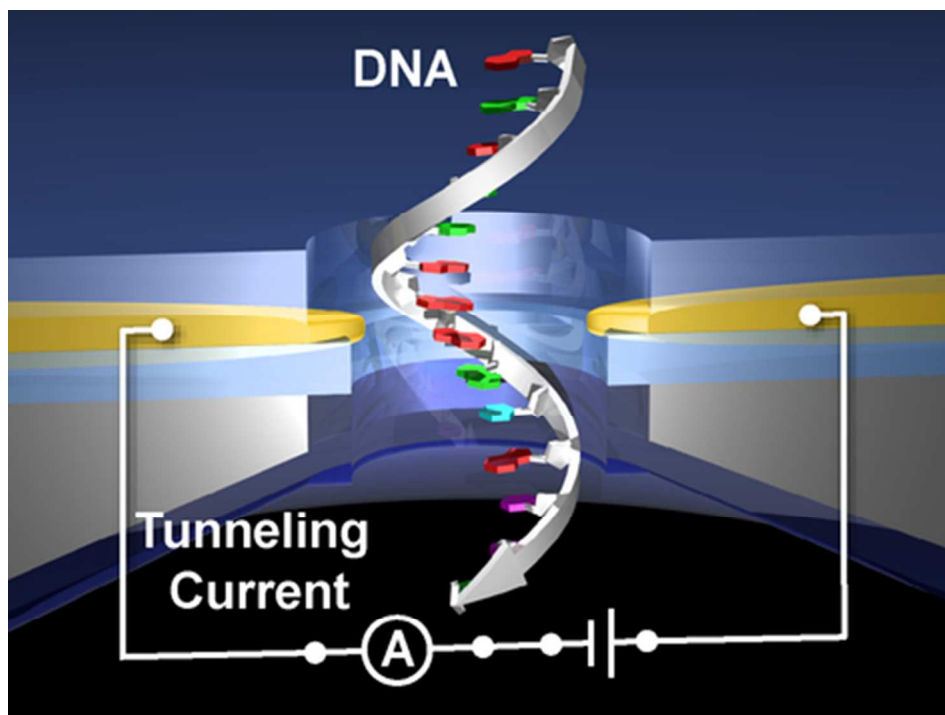
Notes and references

The Institute of Scientific and Industrial Research, Osaka University. 8-1 Mihogaoka, Ibaraki, Osaka 567-0047, Japan.

- F. S. Collins, E. D. Green, A. E. Gutmacher and M. S. Guyer, *Nature*, 2003, **422**, 1.
- J. A. Schloss, *Nat. Biotechnol.*, 2008, **26**, 1113.
- L. Liu, Y. Li, S. Li, N. Hu, Y. He, R. Pong, D. Lin, L. Lu and M. Law, *J. Biomed. Biotechnol.*, 2012, **2012**, 251364.
- D. Branton, D. W. Deamer, A. Marziali, H. Bayley, S. A. Benner, T. Butler, M. Di Ventra, S. Garaj, A. Hibbs, X. Huang, S. B. Jovanovich, P. S. Krstic, S. Lindsay, X. S. Ling, C. H. Mastrangelo, A. Meller, J. S. Oliver, Y. V. Pershin, J. M. Ramsey, R. Riehn, G. V. Soni, V. Tabard-Cossa, M. Wanunu, M. Wiggin and J. A. Schloss, *Nat. Biotechnol.*, 2008, **26**, 1146.
- J. J. Kasianowicz, E. Brandin, D. Branton and D. W. Deamer, *Proc. Natl. Acad. Sci. USA*, 1996, **93**, 13770.
- C. Schmidt, M. Mayer and H. Vogel, *Angew. Chem. Int. Edn.*, 39, **2000**, 3137.
- N. Fertig, Ch. Meyer, R. H. Blick, Ch. Trautmann and J. C. Behrends, *Phys. Rev. E*, 2001, **64**, 040901.
- E. Shafir, H. Cohen, A. Calzolari, C. Cavazzoni, D. A. Ryndyk, G. Cuniberti, A. Kotlyar, R. D. Felice and D. Porath, *Nat. Mater.*, 7, 2008, 68.
- S. Chang, J. He, A. Kibel, M. Lee, O. Sankey, P. Zhang and S. Lindsay, *Nat. Nanotechnol.*, 2009, **4**, 297.
- M. Tsutsui, M. Taniguchi, K. Yokota and T. Kawai, *Nat. Nanotechnol.*, 2010, **5**, 286.
- B. M. Venkatesan and R. Bashir, *Nat. Nanotechnol.*, 2011, **6**, 615.
- S. Weiss, *Science*, 1999, **283**, 1676.
- J. Li, D. Stein, C. McMullan, D. Branton, M. J. Aziz and J. A. Golovchenko, *Nature*, 2001, **412**, 166.
- J. E. Hall, *J. Gen. Physiol.*, 1975, **66**, 531.
- L. Bacri, A. G. Oukhaled, B. Schiedt, G. Patriarche, E. Bourhis, J. Gierak, J. Pelta and L. Auvray, *J. Phys. Chem. B*, 2011, **115**, 2890.
- R. W. DeBlois and C. P. Bean, *Rev. Sci. Instrum.*, 1970, **41**, 909.
- J. Li, M. Gershow, D. Stein, E. Brandin and J. A. Golovchenko, *Nat. Mater.*, 2003, **2**, 611.
- A. J. Storm, J. H. Chen, H. W. Zandbergen and C. Dekker, *Phys. Rev. E*, 2005, **71**, 051903.
- A. J. Storm, C. Storm, J. Chen, H. Zandbergen, J.-F. Joanny and C. Dekker, *Nano Lett.*, 2005, **5**, 1193.
- M. Wanunu, T. Dadosh, V. Ray, J. Jin, L. McReynolds and M. Drndić, *Nat. Nanotechnol.*, 2010, **5**, 807.
- B. M. Venkatesan, B. Dorvel, S. Yemencioğlu, N. Watkins, I. Petrov and R. Bashir, *Adv. Mater.*, 2009, **21**, 2771.
- S. Garaj, W. Hubbard, A. Reina, J. Kong, D. Branton and J. A. Golovchenko, *Nature*, 2010, **467**, 190.
- S. W. Kowalczyk, A. Y. Grosberg, Y. Rabin and C. Dekker, *Nanotechnology*, 2011, **22**, 315101.
- M. Pevarnik, K. Healy, M. E. Toimil-Molaes, A. Morrison, S. E. Létant and Z. S. Siwy, *ACS Nano*, 2012, **6**, 7295.
- R. M. M. Smeets, U. F. Keyser, D. Krapf, M.-Y. Wu, N. H. Dekker and C. Dekker, *Nano Lett.*, 2006, **6**, 89.
- D. Stein, M. Kruithof and C. Dekker, *Phys. Rev. Lett.*, 2004, **93**, 035901.
- R. B. Schoch and P. Renaud, *Appl. Phys. Lett.*, 2005, **86**, 253111.
- R. B. Schoch, J. Han and P. Renaud, *Rev. Mod. Phys.*, 2008, **80**, 839.
- A. Siria, P. Ponchara, A.-L. Biance, R. Fulcrand, X. Blase, S. T. Purcell and L. Bocquet, *Nature*, 2013, **494**, 455.
- H. Chang, F. Kosari, G. Andreadakis, M. A. Alam, G. Vasmatzis and R. Bashir, *Nano Lett.*, 2004, **4**, 1551.
- S. W. Kowalczyk and C. Dekker, *Nano Lett.*, 2012, **12**, 4159.
- Y. He, M. Tsutsui, C. Fan, M. Taniguchi, and T. Kawai, *ACS Nano*, 2011, **5**, 5509.
- Y. He, M. Tsutsui, C. Fan, M. Taniguchi, and T. Kawai, *ACS Nano*, 2011, **5**, 8391.
- R. Karnik, R. Fan, M. Yue, D. Li, P. Yang and A. Majumdar, *Nano Lett.*, 2005, **5**, 943.
- S.-W. Nam, M. J. Rooks, K.-B. Kim and S. M. Rossnagel, *Nano Lett.*, 2009, **9**, 2044.
- X. Liang and S. Y. Chou, *Nano Lett.*, 2008, **8**, 1472.
- A. Rutkowska, J. B. Edell and T. Albrecht, *ACS Nano*, 2013, **7**, 547.
- L. D. Menard, C. E. Mair, M. E. Woodson, J. P. Alarie and J. M. Ramsey, *ACS Nano*, 2012, **6**, 9087.
- J. Wilson and M. Di Ventra, *Nanotechnology*, 2013, **24**, 415101.
- A. Leroux, J. Destiné, B. Vanderheyden, M. E. Gracheva, and J.-P. Leburton, *IEEE Trans. Nanotechnol.*, 2010, **9**, 322.
- R. J. Abraham and P. E. Smith, *Nucleic Acids Res.*, 1998, **16**, 2639.
- J. Sponer, J. Leszczynski, and P. Hobza, *Biopolymers*, 2002, **61**, 3.

- 43 J. B. Heng, A. Aksimentiev, C. Ho, V. Dimitrov, T. W. Sorsch, J. F. Miner, W. M. Mansfield, K. Schulten and G. Timp, *Bell Labs Tech. J.*, 2005, **10**, 5.
- 44 M. E Gracheva, A. Xiong, A. Aksimentiev, K. Schulten, G. Timp and J.-P. Leburton, *Nanotechnology*, 2006, **17**, 622.
- 45 G. Sigalov, J. Comer, G. Timp and A. Aksimentiev, *Nano Lett.*, 2008, **8**, 56.
- 46 A. Leroux, J. Destin e, B. Vanderheyden, M. E. Gracheva and J.-P. Leburton, *IEEE Trans. Nanotechnol.*, 2010, **9**, 322.
- 47 P. Xie, Q. Xiong, Y. Fang, Q. Qing and C. M. Lieber, *Nat. Nanotechnol.*, 2012, **7**, 119.
- 48 F. Traversi, C. Raillon, S. M. Benameur, K. Liu, S. Khlybov, M. Tosun, D. Krasnozhan, A. Kis and A. Radenovic, *Nat. Nanotechnol.*, 2013, **8**, 939.
- 49 M. Puster, J. A. Rodr guez-Manzo, A. Balan and M. Drndi c, *ACS Nano*, 2013, **7**, 11283.
- 50 T. Nelson, B. Zhang and O. V. Prezhdo, *Nano Lett.*, 2010, **10**, 3237.
- 51 K. K. Saha, M. Drndi c and B. K. Nikoli c, *Nano Lett.*, 2012, **12**, 50.
- 52 M. Zwolak and M. Di Ventra, *Rev. Mod. Phys.* 2008, **80**, 141.
- 53 M. Zwolak and M. Di Ventra, *Nano Lett.*, 2005, **5**, 421.
- 54 H. Tanaka and T. Kawai, *Nat. Nanotechnol.*, 2009, **4**, 518.
- 55 J. Lagerqvist, M. Zwolak and M. Di Ventra, *Nano Lett.*, 2006, **4**, 779.
- 56 M. Krems, M. Zwolak, Y. V. Pershin and M. Di Ventra, *Biophys. J.*, 2009, **97**, 1990.
- 57 J. Lagerqvist, M. Zwolak and M. Di Ventra, *Biophys. J.*, 2007, **93**, 2384.
- 58 H. He, R. H. Scheicher, R. Pandey, A. R. Rocha, S. Sanvito, A. Grigoriev, R. Ahuja, S. P. Karna, *J. Phys. Chem. C*, 2008, **112**, 3456–3459.
- 59 X. Chen, *Appl. Phys. Lett.*, 2013, **103**, 063306.
- 60 X. Chen, *Int. J. Quantum Chem.*, 2013, **113**, 2295.
- 61 X. Chen, I. Rungger, C. D. Pemmaraju, U. Schwingenschl g and S. Sanvito, *Phys. Rev. B*, 2012, **85**, 115436.
- 62 H. W. Ch. Postma, *Nano Lett.*, 2010, **10**, 420.
- 63 J. Prasongkit, A. Grigoriev, B. Pathak, R. Ahuja and R. H. Scheicher, *Nano Lett.*, 2011, **11**, 1941.
- 64 B. C. Gierhart, D. G. Howitt, S. J. Chen, Z. Zhud, D. E. Kotecki, R. L. Smith and S. D. Collins, *Sens. Actuator B-Chem.*, 2008, **132**, 593.
- 65 M. Taniguchi, M. Tsutsui, K. Yokota and Tomoji Kawai, *Appl. Phys. Lett.* 2009, **95**, 123701.
- 66 K. Healy, V. Ray, L. J. Willis, N. Peterman, J. Bartel and M. Drndi c, *Electrophoresis*, 2012, **33**, 3488.
- 67 A. Fanget, F. Traversi, S. Khlybov, P. Granjon, A. Magrez, L. Forr o and A. Radenovic, *Nano Lett.*, 10.1021.
- 68 Z. Jiang, M. Mihovilovic, J. Chan and D. Stein, *J. Phys.-Condes. Matter*, 2010, **22**, 454114.
- 69 A. P. Ivanov, E. Instuli, C. M. McGilvery, G. Baldwin, D. W. McComb, T. Albrecht and J. B. Edell, *Nano Lett.*, 2011, **11**, 279.
- 70 C. Hamai, H. Tanaka and T. Kawai, *J. Phys. Chem. B*, 2000, **104**, 9894.
- 71 B. Xu and N. J. Tao, *Science*, 2003, **301**, 1221.
- 72 M. A. Reed, C. Zhou, C. J. Muller, T. P. Burgin and J. M. Tour, *Science*, 1997, **278**, 252.
- 73 M. Tsutsui, K. Matsubara, T. Ohshiro, M. Furuhashi, M. Taniguchi and T. Kawai, *J. Am. Chem. Soc.*, 2011, **133**, 9124.
- 74 T. Ohshiro, K. Matsubara, M. Tsutsui, M. Furuhashi, M. Taniguchi and T. Kawai, *Sci. Rep.*, 2012, **2**, 501.
- 75 M. Tsutsui, S. Rahong, Y. Iizumi, T. Okazaki, M. Taniguchi and T. Kawai, *Sci. Rep.*, 2011, **1**, 46.
- 76 S. Chang, S. Huang, J. He, F. Liang, P. Zhang, S. Li, X. Chen, O. Sankey and S. Lindsay, *Nano Lett.*, 2010, **10**, 1070.
- 77 S. Huang, J. He, S. Chang, P. Zhang, F. Liang, S. Li, M. Tuchband, A. Fuhrmann, R. Ros and S. Lindsay, *Nat. Nanotechnol.*, 2010, **5**, 868.
- 78 M. Tsutsui, Y. He, M. Furuhashi, S. Rahong, M. Taniguchi and T. Kawai, *Sci. Rep.*, 2012, **2**, 394.
- 79 L. D. Menard, C. E. Mair, M. E. Woodson, J. P. Alarie and J. M. Ramsey, *ACS Nano*, 2012, **6**, 9087.
- 80 B. H. Davis, J. Pan, C. –K. Tung, R. B. Austin and R. Riehn, *Nano LIFE*, 2013, **3**, 1340007.
- 81 L. Lesser-Rojas, K. K. Sriram, K. –T. Liao, S. –C. Lai, P. –C. Kuo, M. –L. Chu and C. –F. Chou, *AIP Biomicrofluidics*, 2014, **8**, 016501.
- 82 J. Wilson and M. Di Ventra, *Nanotechnology*, 2013, **24**, 415101.
- 83 K. K. Saha, M. Drndic and B. K. Nikoli c, *Nano Lett.*, 2012, **12**, 50.
- 84 U. F. Keyser, *J. R. Soc. Interface*, 2011, **8**, 1369.
- 85 Y. He, M. Tsutsui, M. Taniguchi and T. Kawai, *J. Mater. Chem.* 2012, **22**, 13423.
- 86 A. J. Storm, C. Storm, J. Chen, H. Zandbergen, J. –F. Joanny and C. Dekker, *Nano Lett.*, 2005, **5**, 1193.
- 87 C. Dekker, *Nat. Nanotechnol.* 2007, **2**, 209.
- 88 G. F. Schneider and C. Dekker, *Nat. Biotechnol.* 2012, **30**, 326.
- 89 J. K. Rosenstein, M. Wanunu, C. A. Merchant, M. Drndic and K. L. Shepard, *Nat. Methods*, 2012, **9**, 487.
- 90 C. A. Merchant, K. Healy, M. Wanunu, V. Ray, N. Peterman, J. Bartel, M. D. Fischbein, K. Ventra, Z. Luo, A. T. C. Johnson and M. Drndic, *Nano Lett.* 2010, **10**, 2915.
- 91 G. F. Schneider, S. W. Kowalczyk, V. E. Calado, G. Pandraud, H. W. Zandbergen, L. M. K. Vandersypen and C. Dekker, *Nano Lett.*, 2010, **10**, 3163.
- 92 S. Garaj, W. Hubbard, A. Reina, J. Kong, D. Branton and J. A. Golovchenko, *Nature*, 2010, **467**, 190.
- 93 M. Muthukumar, *Ann. Rev. Biophys. Biomol. Struct.*, 2007, **36**, 435.
- 94 A. Meller, L. Nivon and D. Branton, *Phys. Rev. Lett.*, **86**, 3435.
- 95 D. Fologea, J. Uplinger, B. Thomas, D. S. McNabb and J. Li, *Nano Lett.*, 2005, **5**, 1734.
- 96 R. M. M. Smeets, U. F. Keyser, D. Krapf, M. –Y. Wu, N. H. Dekker and C. Dekker, *Nano Lett.*, 2006, **6**, 89.
- 97 S. Ghosal, *Phys. Rev. Lett.*, 2007, **98**, 238104.
- 98 M. Wanunu, W. Morrison, Y. Rabin, A. Y. Grosberg and A. Meller, *Nat. Nanotechnol.*, 2010, **5**, 160.
- 99 M. M. Hatlo, D. Panja and R. van Roji, *Phys. Rev. Lett.*, 2011, **107**, 068101.
- 100 T. Chou, *J. Chem. Phys.*, **2009**, 131, 034703.
- 101 Y. He, M. Tsutsui, R. H. Scheicher, C. Fan, M. Taniguchi and T. Kawai, *Biophys. J.*, 2013, **105**, 776.
- 102 L. H. Thamdrupe, N. B. Larsen and A. Kristensen, *Nano Lett.*, 2010, **10**, 826.
- 103 Y. He, M. Tsutsui, R. H. Scheicher, F. Bai, M. Taniguchi and T. Kawai, *ACS Nano*, 2013, **7**, 538.

- 104 M. Belkin, C. Maffeo, D. B. Wells and A. Aksimentiev, *ACS Nano*, 2013, **7**, 6816.
- 105 E. C. Yusko, J. M. Johnson, S. Majd, P. Prangkio, R. C. Rollings, J. Li, J. Yang and M. Nayer, *Nat. Nanotechnol.*, 2011, **6**, 253.
- 106 S. van Dorp, U. F. Keyser, N. H. Dekker, C. Dekker and S. G. Lemay, *Nat. Phys.*, 2009, **5**, 347.
- 107 B. N., Anderson, M. Muthukumar and A. Meller, *ACS Nano*, 2013, **7**, 1408.
- 108 P. Krishnakumar, B. Gyarfas, W. Song, S. Sen, P. Zhang, P. Krstić and S. Lindsay, *ACS Nano*, 2013, **7**, 10319.
- 109 K. R. Lieberman, G. M. Cherf, M. J. Doody, F. Olasagasti, Y. Kolodji and M. Akeson, *J. Am. Chem. Soc.*, 2010, **132**, 17961.
- 110 G. M. Cherf, K. R. Lieberman, H. Rashid, C. E. Lam, K. Karplus and M. Akeson, *Nat. Biotechnol.*, 2012, **30**, 344.
- 111 S. Polonsky, S. Rossnagel and G. Stolovitzky, *Appl. Phys. Lett.*, 2007, **91**, 153103.
- 112 B. Luan, H. Peng, S. Polonsky, S. Rossnagel, G. Stolovitzky and G. Martyna, *Phys. Rev. Lett.*, 2010, **104**, 238103.
- 113 B. Luan, G. Martyna and G. Stolovitzky, *Biophys. J.*, 2011, **101**, 2214.
- 114 Y. Al, J. Liu, B. Zhang and S. Qian, *Anal. Chem.*, 2010, **82**, 8217.
- 115 Y. He, M. Tsutsui, C. Fan, M. Taniguchi and T. Kawai, *ACS Nano*, 2011, **5**, 5509.
- 116 Y. He, M. Tsutsui, C. Fan, M. Taniguchi and T. Kawai, *ACS Nano*, 2011, **5**, 8391.
- 117 P. -C. Yen, C. -H. Wang, G. -J. Hwang and Y. C. Chou, *Rev. Sci. Instrum.*, 2012, **83**, 034301.
- 118 J. R. Moffitt, Y. R. Chemla, S. B. Smith and C. Bustamante, *Annu. Rev. Biochem.*, 2008, **77**, 205.
- 119 U. F. Keyser, B. N. Koeleman, S. van Dorp, D. Krapf, R. M. M. Smeets, S. G. Lemay, N. H. Dekker and C. Dekker, *Nat. Phys.*, 2006, **2**, 473.
- 120 M. van den Hout, I. D. Vilfan, S. Hage and N. H. Dekker, *Nano Lett.*, 2010, **10**, 701.
- 121 W. -J. Lan, D. A. Holden, J. Liu and H. S. White, *J. Phys. Chem. C*, 2011, **115**, 18445.
- 122 B. Lu, D. P. Hoogerheide, Q. Zhao, H. Zhang, Z. Tang, D. Yu and J. A. Golovchenko, *Nano Lett.*, 2013, **13**, 3048.
- 123 U. Mirsaidov, J. Comer, V. Dimitrov, A. Aksimentiev and G. Timp, *Nanotechnology*, 2010, **21**, 395501.
- 124 V. Kurz, E. M. Nelson, J. Shim and G. Timp, *ACS Nano*, 2013, **7**, 4057.
- 125 M. Wanunu, J. Sutin, B. McNally, A. Chow, and A. Meller, *Biophys. J.*, 2008, **95**, 4716.
- 126 S. Garaj, S. Sliu, J. A. Golovchenko and D. Branton, *Proc. Natl. Acad. Sci.*, 2013, **110**, 12192.



Electrode-embedded nanopores have been developed to realize label-free, low-cost, and high-throughput DNA sequencers.
39x29mm (300 x 300 DPI)